IOPscience iopscience.iop.org

Home Search Collections Journals About Contact us My IOPscience

Application of magnetic resonance force microscopy cyclic adiabatic inversion for a single-spin measurement

This article has been downloaded from IOPscience. Please scroll down to see the full text article.

2003 J. Phys. A: Math. Gen. 36 4417

(http://iopscience.iop.org/0305-4470/36/15/314)

View the table of contents for this issue, or go to the journal homepage for more

Download details:
IP Address: 171.66.16.96
The article was downloaded on 02/06/2010 at 11:36

Please note that terms and conditions apply.

INSTITUTE OF PHYSICS PUBLISHING JOURNAL OF PHYSICS A: MATHEMATICAL AND GENERAL

J. Phys. A: Math. Gen. **36** (2003) 4417–4432 PII: S0305-4470(03)39284-4

Application of magnetic resonance force microscopy cyclic adiabatic inversion for a single-spin measurement

G P Berman[1], F Borgonovi[1,2,3,4], G Chapline[1,5], S A Gurvitz[1,6], P C Hammel[7], D V Pelekhov[7], A Suter[7] and V I Tsifrinovich[8]

[1] Theoretical Division and CNLS, Los Alamos National Laboratory, Los Alamos, NM 177545, USA
[2] Dipartimento di Matematica e Fisica, Università Cattolica, via Trieste 17, 25121 Brescia, Italy
[3] INFN, Sezione di Pavia, Italy
[4] INFM, Unità di Brescia, Italy
[5] Lawrence Livermore National Laboratory, Livermore, CA 94551, USA
[6] Department of Particle Physics, Weizmann Institute of Sciences, Rehovot 76100, Israel
[7] MST-10, Los Alamos National Laboratory, MS K764, Los Alamos, NM 87545, USA
[8] IDS Department, Polytechnic University, Six Metrotech Center, Brooklyn, NY 11201, USA

Received 9 July 2002, in final form 26 February 2003
Published 3 April 2003
Online at stacks.iop.org/JPhysA/36/4417

Abstract

We consider the process of a single-spin measurement using magnetic resonance force microscopy (MRFM) with a cyclic adiabatic inversion (CAI). This technique is also important for different applications, including a measurement of a qubit state in quantum computation. The measurement takes place through the interaction of a single spin with a cantilever modelled by a quantum oscillator in a coherent state in a quasi-classical range of parameters. The entire system is treated rigorously within the framework of the Schrödinger equation. For a many-spin system our equations accurately describe conventional MRFM experiments involving CAI of the spin system.

Our computer simulations of the quantum spin–cantilever dynamics show that the probability distribution for the cantilever position develops two asymmetric peaks with the total relative probabilities mainly dependent on the initial angle between the directions of the average spin and the effective magnetic field, in the rotating frame. We show that each of the peaks is correlated with the direction of the average spin (being along or opposite to the direction of the effective magnetic field). This generates two possible outcomes of a single-spin measurement, similar to the Stern–Gerlach effect. We demonstrate that the generation of the second peak can be significantly suppressed by turning on adiabatically the amplitude of the rf magnetic field. We also show that MRFM CAI can be used both for detecting a signal from a

 © 2003 IOP Publishing Ltd Printed in the UK

single spin, and for measuring the single-spin state by measuring the phase of the cantilever driving oscillations.

PACS numbers: 03.67.Lx, 03.67.−a, 76.60.−k

1. Introduction

The problem of detecting a signal from a single electron and nuclear spin is extremely important for successful development of future quantum technologies. One of these technologies is quantum computation (see, for example, [1–6]). In solid-state quantum computers, a single quantum bit (qubit) can be realized using different quantum two-level systems [7]. In particular, a qubit can be represented by a nuclear [8, 9] or an electron [10–13] spin. To extract the information from a quantum computer one must read out a state of a single qubit. This means that one must at least measure a signal from a magnetic moment produced by a single spin. Recently, there exist different proposals to realize a single-spin quantum measurement (see, for example, [8, 9, 12, 14]). One of them is based on magnetic resonance force microscopy (MRFM).

MRFM was first proposed by Sidles in 1991 as a sensitive method to detect a signal from small magnetic samples [15]. Since this time, MRFM has been successfully used to increase the sensitivity and spatial resolution for electron spin resonance [16], ferromagnetic resonance [17], and nuclear magnetic resonance [18]. For a recent review on MRFM see [19].

In conventional MRFM (see figure 1), a magnetic particle produces a non-uniform magnetic field which attracts or repels the magnetic moment of a sample placed, in our case, on a cantilever tip, depending on the direction of a magnetic moment. The magnetic resonance technique in MRFM CAI provides two types of magnetic moment oscillation in the reference frame which rotates with the rf field: the fast oscillation around the effective magnetic field, and the slow oscillation with the cantilever frequency. These oscillations cause resonant vibrations of the cantilever that can be detected, for example, using optical methods.

We would also like to mention here a connection between the MRFM CAI and the problem of a 'continuous' measurement of a quantum system which means a continuous monitoring of the dynamics of a macroscopic system caused by the dynamics of a quantum system (see, for example, [20, 21]).

As a necessary step to approach the problems of a single-spin measurement using MRFM CAI we perform a detailed quantum mechanical analysis of the coupling of a single spin to a cantilever. We treat the measurement device (a quasi-classical cantilever) entirely quantum mechanically together with a single spin as an isolated quantum system described by the Schrödinger equation.

This pure quantum mechanical approach allows us to answer the following crucial question: what spin projection is measured by a cantilever in MRFM CAI? Namely, in a *standard* Stern–Gerlach experiment one measures the spin projection along the direction of the magnetic field (the z-direction). At the same time, in the classical version of MRFM CAI the magnetic moment of the sample is oriented along the direction of the effective magnetic field that oscillates in the rotating reference frame (x–z plane). So, the central question is whether in the quantum case the *natural* axis of the spin quantization is the direction of the cantilever oscillations (the z-direction) or the direction of the oscillating magnetic field. Our numerical simulations demonstrate that under the parameters used in MRFM CAI the axis of

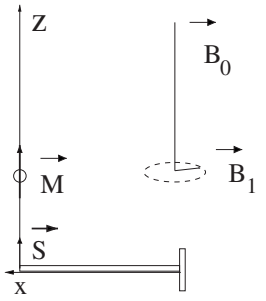

Figure 1. A schematic set-up of the spin–cantilever system. $\vec{B}_0$ is the uniform permanent magnetic field oriented in the positive z-direction; $\vec{B}_1$ is the rotating magnetic field; $\vec{S}$ is a single spin ($S = 1/2$); $\vec{M}$ is the magnetic moment of the ferromagnetic particle.

spin quantization is the direction of the oscillating effective magnetic field. This conclusion is important because it means that the quantum version of MRFM CAI (in which a spin is supposed to rotate fast around the effective magnetic field and to follow its oscillations adiabatically) can be realized.

In section 2 we formulate the classical problem of the driven oscillations of the cantilever. We then present its quantum mechanical equivalent for a spin–cantilever system in the Schrödinger representation. The cantilever is prepared initially in a quantum coherent state using parameters that place it in a quasi-classical regime. We show that these parameters in the classical limit of a many-spin system correspond to real experimental conditions of CAI. In section 3 we consider the quantum dynamics of a single spin–cantilever system when the spin is rotated by CAI. Our computer simulations explicitly demonstrate the formation of two distinctive peaks in the probability distribution of the cantilever position. These two peaks are quasi-periodically overlapping with a period which matches that of the CAI of the spin. In section 4 we show that each of the two peaks in the cantilever distribution involves a superposition of both the stationary spin states. The average spin in one of the peaks is oriented approximately in the direction of the effective magnetic field (in the rotating reference frame), and in the other peak the average spin is oriented approximately in the direction opposite to the direction of the effective magnetic field. This results in an unwanted effect—two possible outcomes (quantum jump) of a single-spin measurement (similar to the Stern–Gerlach effect). We show that turning on adiabatically the amplitude of the rf magnetic field can significantly suppress the magnitude of one of the peaks ($\sim 10^{-6}$ for chosen parameters). As shown in section 5, this will allow one to use MRFM CAI not only for detecting a signal from a single spin, but also for measuring a single-spin state by measuring the phase of the cantilever driving oscillations. The summary of our results is presented in section 6.

2. Formulation of the model

Consider the cantilever–spin system shown in figure 1, namely, a single spin ($S = 1/2$) is placed on the cantilever tip. The tip can oscillate only in the z-direction. The ferromagnetic particle, whose magnetic moment points in the positive z-direction, produces a non-uniform magnetic field at the spin. The uniform magnetic field, $\vec{B}_0$, oriented in the positive z-direction, determines the ground state of the spin. The rotating magnetic field, $\vec{B}_1$, induces transitions between the ground and the excited states of the spin. The origin is chosen to be the equilibrium

position of the cantilever tip with no ferromagnetic particle. The rotating magnetic field can be represented as

$$B_x = B_1 \cos(\omega t + \varphi(t)) \qquad B_y = -B_1 \sin(\omega t + \varphi(t)) \tag{1}$$

where $\varphi(t)$ describes a smooth change in phase required for a cyclic adiabatic inversion (CAI) of the spin ($|\mathrm{d}\varphi/\mathrm{dt}| \ll \omega$).

The classical motion for the cantilever displacement, $Z(x = l_c, t)$ (where x is the coordinate along the cantilever and l_c the length of the cantilever), under the action of the 'effective external harmonic force' (EEHF), $F_\omega \, \mathrm{e}^{\mathrm{i}\omega t}$, takes the form [22]

$$Z = \frac{4}{m_c} \sum_{n=1}^{\infty} \frac{F_\omega}{\omega_n^2 - \omega^2} \, \mathrm{e}^{\mathrm{i}\omega t} \tag{2}$$

where m_c is the mass of the cantilever. The summation in equation (2) is taken over all eigen-frequencies of the cantilever. Neglecting all terms in equation (2) except for the first one with $n = 1$, and taking into consideration the finite value of the quality factor, Q, of the cantilever, we have from equation (2)

$$Z \approx \frac{4F_\omega/m_c}{\omega_c^2 - \omega^2 + 2\mathrm{i}\omega^2/\mathrm{Q}} \, \mathrm{e}^{\mathrm{i}\omega \mathrm{t}} \tag{3}$$

where ω_c is the lowest eigen-frequency of the cantilever.

Equation (3) describes the resonant enhancement of the classical oscillations by a quality factor, Q. For the corresponding quantum mechanical treatment of the same cantilever–spin system we introduce the Hamiltonian in the reference frame rotating with $\vec{B}_1$,

$$\mathcal{H} = \frac{P_z^2}{2m_c^*} + \frac{m_c^* \omega_c^2 Z^2}{2} - \hbar \left(\omega_L - \omega - \frac{\mathrm{d}\varphi}{\mathrm{d}t} \right) S_z - \hbar \omega_1 S_x - g\mu \frac{\partial B_z}{\partial Z} Z S_z \tag{4}$$

where we defined $m_c^* = m_c/4$ as the effective cantilever mass. In equation (4), Z is the coordinate of the oscillator which describes the dynamics of the cantilever tip; P_z is its momentum,

$$\omega_c = (k_c/m_c^*)^{1/2} \qquad \omega_L = \gamma B_z \qquad \omega_1 = \gamma B_1 \tag{5}$$

where B_z includes the uniform magnetic field, B_0, and the magnetic field produced by the ferromagnetic particle at the spin location (at $z = 0$); $\gamma = g\mu/\hbar$ is the gyromagnetic ratio of the spin; S_z and S_x are the z- and the x-components of the spin; ω_L is its Larmor frequency; ω_1 is the Rabi frequency (the frequency of the spin precession around the field B_1 at the resonance: $\omega = \omega_L, \dot{\varphi} = 0$); g and μ are the g-factor and the nuclear magneton (or the Bohr magneton in the case of an electron spin).

It is useful to rewrite the Hamiltonian (4) in the dimensionless form by introducing the following 'quanta' of the oscillator (cantilever): energy (E_0), force (F_0), amplitude (Z_0) and momentum (P_0),

$$E_0 = \hbar\omega_c \qquad F_0 = \sqrt{k_c E_0} \qquad Z_0 = \sqrt{E_0/k_c} \qquad P_0 = \hbar/Z_0. \tag{6}$$

Using these dimensionless quantities and setting $\omega = \omega_L$, Hamiltonian (4) reads

$$\mathcal{H}' = \mathcal{H}/\hbar\omega_c = \left(p_z^2 + z^2\right)/2 + \dot{\varphi} S_z - \varepsilon S_x - 2\eta z S_z \tag{7}$$

where

$$\begin{aligned} &p_z = P_z/P_0 \qquad z = Z/Z_0 \qquad \dot{\varphi} = \mathrm{d}\varphi/\mathrm{d}\tau \qquad \tau = \omega_c t \\ &\varepsilon = \omega_1/\omega_c \qquad \eta = g\mu(\partial B_z/\partial Z)/2F_c. \end{aligned} \tag{8}$$

Here ε and η in equation (8) are two dimensionless parameters which characterize the quantum dynamics described by the Hamiltonian (7). In detail, ε is the dimensionless Rabi frequency, while η is the dimensionless magnetic force produced by a single spin on the cantilever.

To estimate the 'quanta' in (6) and the dimensionless parameters in (8), we use parameters from the MRFM measurement [18] of protons in ammonium nitrate,

$$\begin{aligned} &\omega_c/2\pi = 1.4 \times 10^3 \text{ Hz} && k_c = 10^{-3} \text{ N m}^{-1} \\ &B_1 = 1.2 \times 10^{-3} \text{ T} && \partial B_z/\partial Z = 600 \text{ T m}^{-1} \\ &\gamma/2\pi = 4.3 \times 10^7 \text{ Hz T}^{-1}. \end{aligned} \tag{9}$$

Using these values, we obtain

$$\begin{aligned} &E_0 = 9.2 \times 10^{-31} \text{ J} && F_0 = 3 \times 10^{-17} \text{ N} \\ &Z_0 = 3 \times 10^{-14} \text{ m} && P_0 = 3.5 \times 10^{-21} \text{ kg m s}^{-1} \\ &\varepsilon = 37 && \eta = 2.8 \times 10^{-7}. \end{aligned} \tag{10}$$

The dimensionless Schrödinger equation can be written in the form

$$\mathrm{i}\dot{\Psi} = \mathcal{H}'\Psi \tag{11}$$

where

$$\Psi(z,\tau) = \begin{pmatrix} \psi_1(z,\tau) \\ \psi_2(z,\tau) \end{pmatrix} \tag{12}$$

is a dimensionless spinor, and $\dot{\Psi} = \partial\Psi/\partial\tau$. Next, we expand the functions $\psi_1(z,\tau)$ and $\psi_2(z,\tau)$ in terms of the eigenfunctions, $|n\rangle$, of the unperturbed oscillator Hamiltonian, $\left(p_z^2 + z^2\right)/2$,

$$\begin{aligned} &\psi_1(z,\tau) = \sum_{n=0}^{\infty} A_n(\tau)|n\rangle \qquad \psi_2(z,\tau) = \sum_{n=0}^{\infty} B_n(\tau)|n\rangle \\ &|n\rangle = \pi^{1/4} 2^{n/2} (n!)^{1/2} \, \mathrm{e}^{-z^2/2} H_n(z) \end{aligned} \tag{13}$$

where $H_n(z)$ are the Hermitian polynomials. Substituting (13) in (11) and taking into account (7), we derive the coupled system of equations for the complex amplitudes, $A_n(\tau)$ and $B_n(\tau)$,

$$\begin{aligned} \mathrm{i}\dot{A}_n &= (n + 1/2 + \dot{\varphi}/2)A_n - (\eta/\sqrt{2})\left(\sqrt{n}A_{n-1} + \sqrt{n+1}A_{n+1}\right) - (\varepsilon/2)B_n \\ \mathrm{i}\dot{B}_n &= (n + 1/2 + \dot{\varphi}/2)B_n + (\eta/\sqrt{2})\left(\sqrt{n}B_{n-1} + \sqrt{n+1}B_{n+1}\right) - (\varepsilon/2)A_n. \end{aligned} \tag{14}$$

To derive equation (14), we used the well-known expressions for creation and annihilation operators,

$$\begin{aligned} &a|n\rangle = \sqrt{n}|n-1\rangle \qquad a^\dagger|n\rangle = \sqrt{n+1}|n+1\rangle \\ &\left[\left(p_z^2 + z^2\right)/2\right]|n\rangle = (n + 1/2)|n\rangle \\ &z = (a^\dagger + a)/\sqrt{2} \qquad p_z = \mathrm{i}(a^\dagger - a)/\sqrt{2} \\ &[a, a^\dagger] = 1. \end{aligned} \tag{15}$$

To test our model, we considered the classical limit of the macroscopic number of spins and the classical cantilever. For this purpose, we substitute the operators S_x and S_z by the sums of operators over all spins in the sample. Neglecting the quantum correlation effects we derive the classical equations of motion for the average spin of the sample and for the cantilever:

$$\dot{z} = p_z \qquad \dot{p}_z = -z + 2\eta\Delta N S_z \qquad \dot{\vec{S}} = [\vec{S} \times \vec{b}^{\text{eff}}]. \tag{16}$$

Here $\vec{b}^{\text{eff}}$ is the effective magnetic field with components

$$b_x^{\text{eff}} = \varepsilon \qquad b_y^{\text{eff}} = 0 \qquad b_z^{\text{eff}} = -\ddot{\varphi} + 2\eta z \tag{17}$$

and ΔN is the difference in the population of the ground state and the excited state of the spin system. Then to estimate the amplitude of the stationary vibrations of the cantilever within the Hamiltonian approach, we put $\tau = Q_c$, where Q_c is the quality factor of the cantilever. (The value $\tau = Q_c$ corresponds to the time $t = t_c$, where $t_c = Q_c/\omega_c$ is the time constant of the cantilever.)

Taking parameters from the experiment [18]

$$\Delta N = 2.9 \times 10^9 \qquad Q_c \approx 10^3 \tag{18}$$

we obtain for the stationary amplitude of the cantilever

$$z = \Delta N \eta Q_c \approx 8.1 \times 10^5. \tag{19}$$

The corresponding dimensional value of the amplitude is $Z \approx 24$ nm. The experimental value in [18] is 16 nm, which is close to the estimated value.

3. Quantum dynamics for a single spin–cantilever system

The magnetic force between the cantilever and a single spin is extremely small. To simulate the dynamics of the cantilever driven by a single spin, in reasonable times, we take $\eta = 0.3$. Such a value can already be achieved in the present day experiments by measuring a single electron spin (see, for example, [19]).

To describe the cantilever as a sub-system close to the classical limit, we choose the initial wavefunction of the cantilever in the coherent state, $|\alpha\rangle$, in the quasi-classical region of parameters ($|\alpha|^2 \gg 1$). Namely, the initial wavefunction of the cantilever was taken in the form (12) where

$$\begin{aligned} &\psi_1(z,0) = \sum_{n=0}^{\infty} A_n(0)|n\rangle \qquad \psi_2(z,0) = 0 \\ &A_n(0) = (\alpha^n/\sqrt{n!})\exp(-|\alpha|^2/2). \end{aligned} \tag{20}$$

The initial averages of z and p_z can be represented as

$$\langle z\rangle = \frac{1}{\sqrt{2}}(\alpha^* + \alpha) \qquad \langle p_z\rangle = \frac{\mathrm{i}}{\sqrt{2}}(\alpha^* - \alpha). \tag{21}$$

In all numerical simulations we choose $\alpha = -\sqrt{2} \times 10$, which corresponds to the initial average number of excitations in the cantilever: $n = |\alpha|^2 = 200$.

Note that the value $|\alpha|$ cannot be significantly reduced if we simulate a quasi-classical cantilever. At the same time, increasing $|\alpha|$ increases the number of states, $|n\rangle$, involved in the dynamics which makes the simulations of quantum dynamics more complicated.

We numerically integrated system (14) using a standard Runge–Kutta fourth-order method. We checked the stability of our results increasing the dimension of the oscillator basis (up to 3000 levels) and decreasing the time integration step.

Figure 2 shows the typical probability distribution

$$P(z,\tau) = |\psi_1(z,\tau)|^2 + |\psi_2(z,\tau)|^2 \tag{22}$$

obtained from numerical simulations of equations (14) for six instants of time, τ, and for the parameters $\eta = 0.3$ and $\varepsilon = 400$. (The dimensionless period, $\Delta\tau = 2\pi$, corresponds to the dimensional period, $\Delta t = 2\pi/\omega_c$.) This figure reveals that the cantilever can be found in two different positions. Indeed, near $\tau = 80$, the probability distribution (22) splits into two asymmetric peaks. After this the separation between these two peaks varies periodically in

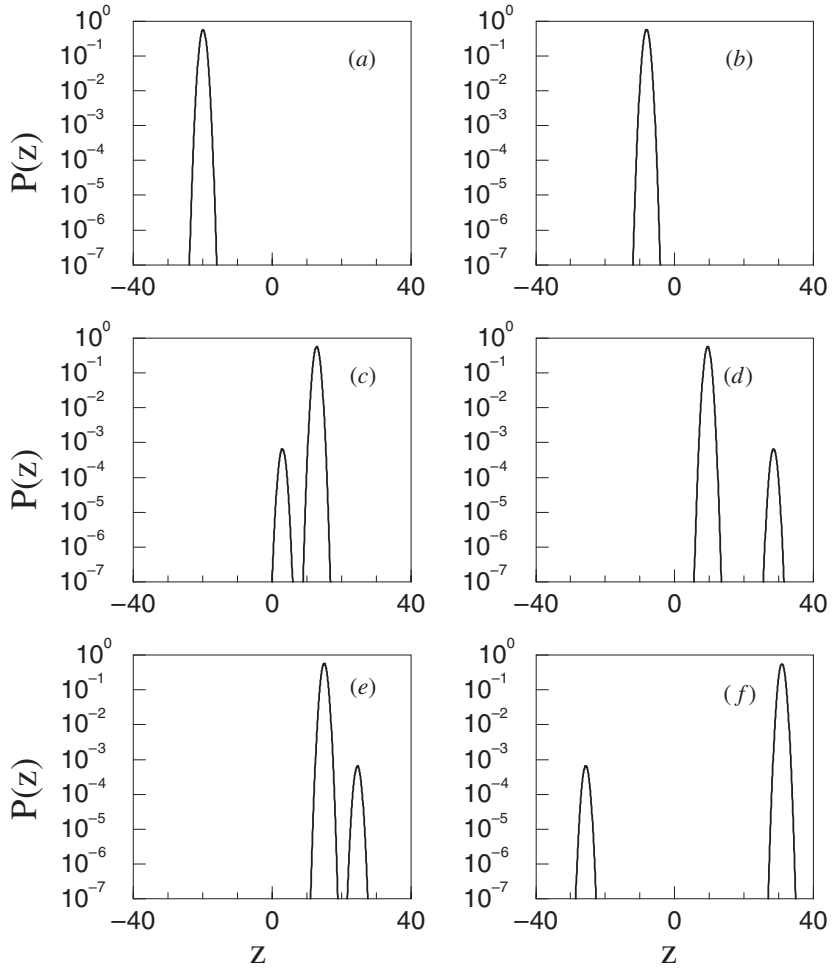

Figure 2. Probability distribution of the cantilever coordinate, z, for $\varepsilon = 400$ and $\eta = 0.3$. The initial conditions: $z(0) \equiv \langle z \rangle = -20$, $p_z(0) \equiv \langle p_z \rangle = 0$ ($\alpha = -\sqrt{2} \times 10$). Times are (*a*) $\tau = 0$, (*b*) $\tau = 20$, (*c*) $\tau = 64.8$, (*d*) $\tau = 104$, (*e*) $\tau = 160$, (*f*) $\tau = 221.6$.

time. The ratio of the peak amplitudes is about 1000 for chosen parameters. (Hence, we show the amplitudes on a logarithmic scale.) The cyclic adiabatic inversion parameters were chosen as

$$\dot{\varphi} = \begin{cases} -6000 + 300\tau & \text{if} \quad \tau \leqslant 20 \\ A \sin(\tau - 20) & \text{if} \quad \tau > 20 \end{cases} \tag{23}$$

where $A = 1000$, so that the standard condition for CAI ($|\ddot{\varphi}| \ll \epsilon^2$) is satisfied. The chosen parameters in equation (23) allow one to 'catch' the spin, initially oriented in the positive (or negative) z-direction, by the effective magnetic field, and to put it approximately in the positive (or negative) x-direction at $\tau = 20$. For times $\tau > 20$, the spin oscillates in the xz-plane, together with the effective magnetic field.

It is clear that the small peak does not significantly influence the average coordinate of the cantilever. Figure 3 shows the average coordinate of the cantilever, $\langle z(\tau) \rangle$, and the corresponding standard deviation, $\Delta(\tau) = [\langle z^2 \rangle - \langle z \rangle^2]^{1/2}$. One can see a fast increase in the

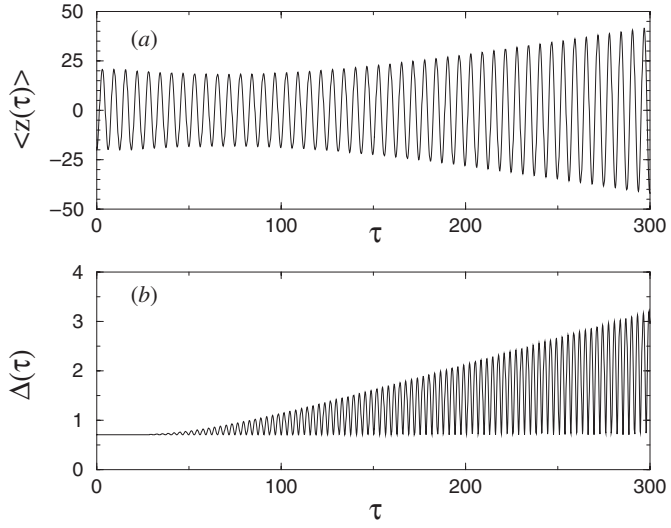

Figure 3. Cantilever dynamics. (*a*) Average coordinate of the cantilever as a function of τ and (*b*) its standard deviation $\Delta(\tau) = [\langle z^2(\tau)\rangle - \langle z(\tau)\rangle^2]^{1/2}$. Data and parameters are the same as in figure 2.

average amplitude of the cantilever vibrations, while the standard deviation still remains small. This, in fact, is related to the initial conditions of the spin, which was taken in the direction of the z-axis. For instance, if the spin initially points in the x-axis ($\psi_1(z, 0) = \psi_2(z, 0)$), our calculations show two large peaks with similar amplitudes.

The two peaks in the cantilever probability distribution, shown in figure 2, indicate two possible trajectories of the cantilever (similar to the Stern–Gerlach effect). As a result of the consequent measurement of the cantilever position the system selects one of the two trajectories.

4. Cantilever–spin entanglement

As shown in figure 2, two asymmetric peaks in the cantilever distribution are well separated for shown instants of time. When the probability distribution splits into these peaks, the distance, d, between them initially increases. Then d decreases so that the two peaks eventually overlap. After this, the probability distribution splits again so that the position of the minor peak is on the opposite side of the major peak. Again the distance, d, first increases, then decreases until the two peaks overlap. This cycle repeats for as long as the simulations are run.

One might expect that the two peaks are associated with the functions $P_n(z, \tau) = |\psi_n(z, \tau)|^2$, $n = 1, 2$. In fact the situation is more subtle: each function $P_n(z, \tau)$ splits into two peaks. Figure 4 shows these two functions for nine instants in time: $\tau_k = 92.08 + 0.8k$, $k = 0, 1, \ldots, 8$ during one period of the cantilever vibration. One can see the splitting of both $P_1(z, \tau)$ and $P_2(z, \tau)$; each peak of the function $P_1(z, \tau)$ has the same position as the two peaks of $P_2(z, \tau)$, but the amplitudes of these peaks differ. For instance, for $k = 1$ ($\tau = 92.88$) the left-hand peak is dominantly composed of $P_1(z, \tau)$, while the right-hand peak is mainly composed of $P_2(z, \tau)$.

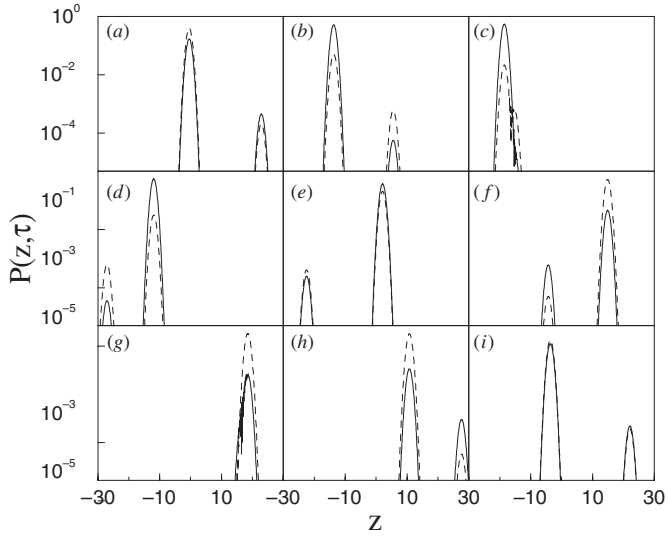

Figure 4. Probability distributions, $P_1(z,\tau) = |\psi_1(z,\tau)|^2$ (solid curves), and $P_2(z,\tau) = |\psi_2(z,\tau)|^2$ (dashed curves) for nine instants of time: $\tau_k = 92.08 + 0.8k$, $k = 0, 1, \ldots, 8$.

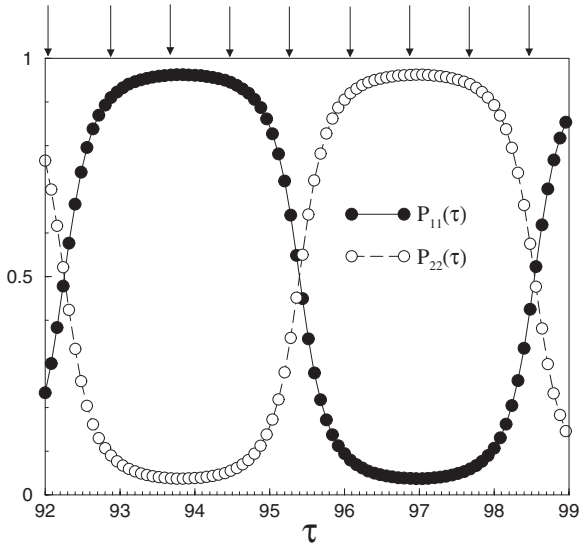

Figure 5. Integrated probability distributions of the spin z-components (diagonal components of the spin density matrix): $P_{11}(\tau)$, for $S_z = 1/2$ (•); and $P_{22}(\tau)$, for $S_z = -1/2$ (○), as functions of time. Vertical arrows show the time instants, $\tau_k = 92.08 + 0.8k$, $k = 0, 1, \ldots, 8$ depicted in figure 4.

Figure 5 shows the spatially integrated probability distributions: $P_{11}(\tau) = \int P_1(z,\tau)\,\mathrm{d}z$ and $P_{22}(\tau) = \int P_2(z,\tau)\,\mathrm{d}z$, as 'truly continuous' functions of time, τ. (Vertical arrows show the time instants, τ_k.)

The crucial problem is the following: do the two peaks of the cantilever distribution correspond to the definite spin states? To answer this question we studied the structure of

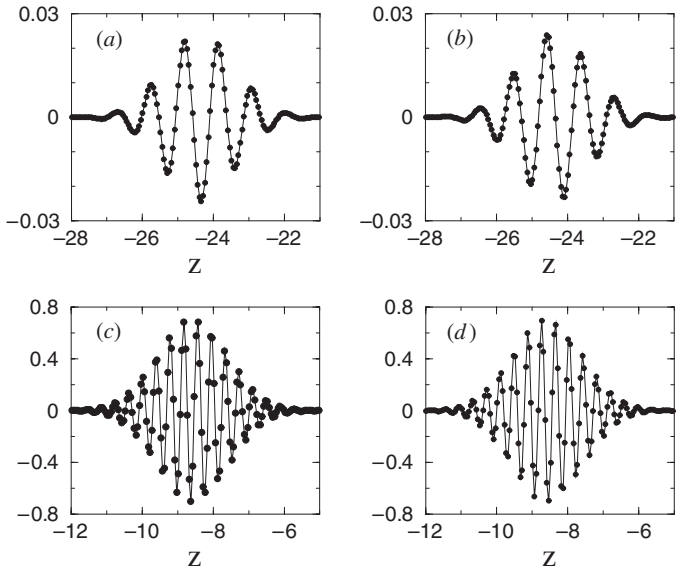

Figure 6. Demonstration of the orthogonality of spin wavefunctions belonging to 'big' and 'small' peaks. (*a*) Circles: $\mathrm{Re}(-\kappa\psi_1^s)$, solid line: $\mathrm{Re}(\psi_2^s)$; (*b*) circles: $\mathrm{Im}(-\kappa\psi_1^s)$, solid line: $\mathrm{Im}(\psi_2^s)$; (*c*) circles: $\mathrm{Re}(\kappa\psi_2^b)$, solid line: $\mathrm{Re}(\psi_1^b)$; (*d*) circles: $\mathrm{Im}(\kappa\psi_2^b)$, solid line: $\mathrm{Im}(\psi_1^b)$, where $\kappa(\tau = 76) = -2.9$.

the wavefunction of the cantilever–spin system. As was already mentioned, both functions, $\psi_1(z, \tau)$ and $\psi_2(z, \tau)$, contribute to each peak (see figure 4). When the two peaks are clearly separated we can represent each of these functions as a sum of two terms, corresponding to the 'big' and 'small' peaks,

$$\psi_{1,2}(z, \tau) = \psi_{1,2}^b(z, \tau) + \psi_{1,2}^s(z, \tau). \tag{24}$$

We have found that with accuracy up to 1% the ratio $\psi_2^s(z, \tau)\big/\psi_1^s(z, \tau) = -\psi_1^b(z, \tau)\big/\psi_2^b(z, \tau) = \kappa(\tau)$, where $\kappa(\tau)$ is a real function independent of z. Results are shown in figure 6, for the same parameter as in figure 2, and for $\tau = 76$ with $\kappa(\tau) = -2.9$ obtained by a best fit procedure.

As a result, the total wavefunction can be represented in the form,

$$\psi(z, s_z, \tau) = \psi^b(z, \tau)\chi^b(s_z, \tau) + \psi^s(z, \tau)\chi^s(s_z, \tau) \tag{25}$$

where $\chi^b(s_z, \tau)$ and $\chi^s(s_z, \tau)$ are spin wavefunctions, which are orthogonal to each other. Equation (25) shows that each peak in the probability distribution of the cantilever coordinate corresponds to a definite spin wavefunction. We found that the average spin, $\langle\chi^b|\vec{S}|\chi^b\rangle$, corresponding to the big peak, points in the direction of the vector $(\epsilon, 0, -\mathrm{d}\varphi/\mathrm{d}\tau)$, whereas the average spin, $\langle\chi^s|\vec{S}|\chi^s\rangle$, corresponding to the small peak, points in the opposite direction. In figure 7, we demonstrate the direction of the effective magnetic field (thick arrow); the direction of the average spin calculated using the $\chi^b(s_z, \tau)$ wavefunction (thin arrow); and the direction of the average spin calculated using the $\chi^s(s_z, \tau)$ wavefunction (thin dashed arrow). This can only be done when the probability distributions corresponding to the small and big peaks, Ψ^b and Ψ^s, are well separated in space. This is not the case in figures 4(*c*) and (*g*). In these cases we represent the total average spin only (as a thin line) (see figures 7(*c*) and (*g*). One should also take into account that the 'lengths' of the effective magnetic field and the average spin of the small head have been renormalized respectively to the lengths 1 and

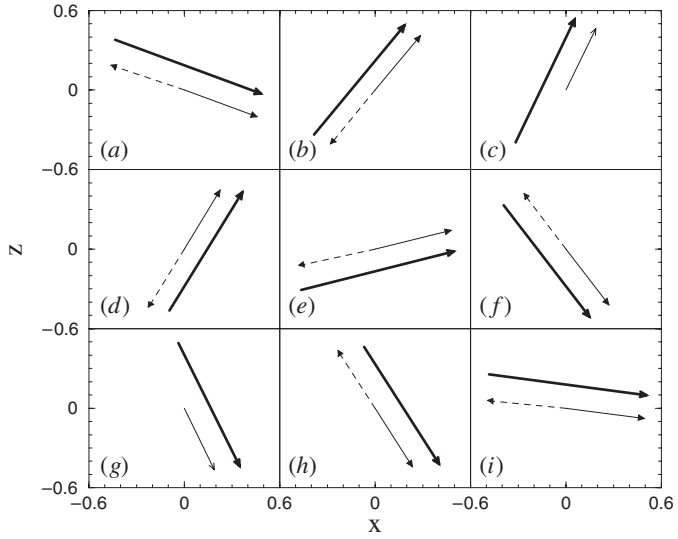

Figure 7. The direction of the effective magnetic field (thick arrow) renormalized to the unit length; the direction of the average spin calculated using the $\chi^b(s_z, \tau)$ wavefunction (thin arrow); and the direction of the average spin calculated using the $\chi^s(s_z, \tau)$ wavefunction (thin dashed arrow) renormalized to the length $1/2$, in order to be plotted in the same picture. Times and parameters as in figure 4. In (*c*) and (*g*) one single thin line has been drawn for the total average spin. This is due to the spatial overlapping of the probability distributions corresponding to the small and big peaks (see text).

$1/2$, in order to put them on the same scale (they are respectively a few order of magnitude larger and smaller than the total average spin). The results presented in figure 7 allow one a better understanding of the structure of the total wavefunction described by equations (24) and (25).

Note that up to a small term, $2\eta z$, the vector

$$(\epsilon, 0, -\mathrm{d}\varphi/\mathrm{d}\tau)$$

is the effective magnetic field acting on the spin. The ratio of the integrated probabilities $\left(\int P(z, \tau)\,\mathrm{d}z\right)$ for the small and big peaks ($\sim 10^{-3}$ in figure 2) can be easily estimated as $\tan^2(\Theta/2)$, where Θ is the initial angle between the effective field, $(\epsilon, 0, -\mathrm{d}\varphi/\mathrm{d}\tau)$, and the spin direction. Therefore, by measuring the cantilever vibrations, one finds the spin in a definite state along or opposite to the effective magnetic field. Our numerical simulations for such a new initial condition, i.e. when the average spin points along or opposite to the effective field, are shown in figure 8. The probability distribution $P(z, \tau)$ again shows two peaks but the ratio of the integrated probabilities of these peaks is much less than in figure 2 ($\sim 10^{-6}$). Note that we used in figure 8 a larger scale on the y-axis than that in figure 2, in order to show that the small peak is clearly beyond the unavoidable numerical errors (below 10^{-25} in figure 8).

Thus for chosen parameters, the probability of the second peak in the cantilever position generated by a single-spin measurement is small. This implies that the appearance of this peak cannot prevent the amplification of the cantilever vibration amplitude, and therefore the measurement of the state of a single spin.

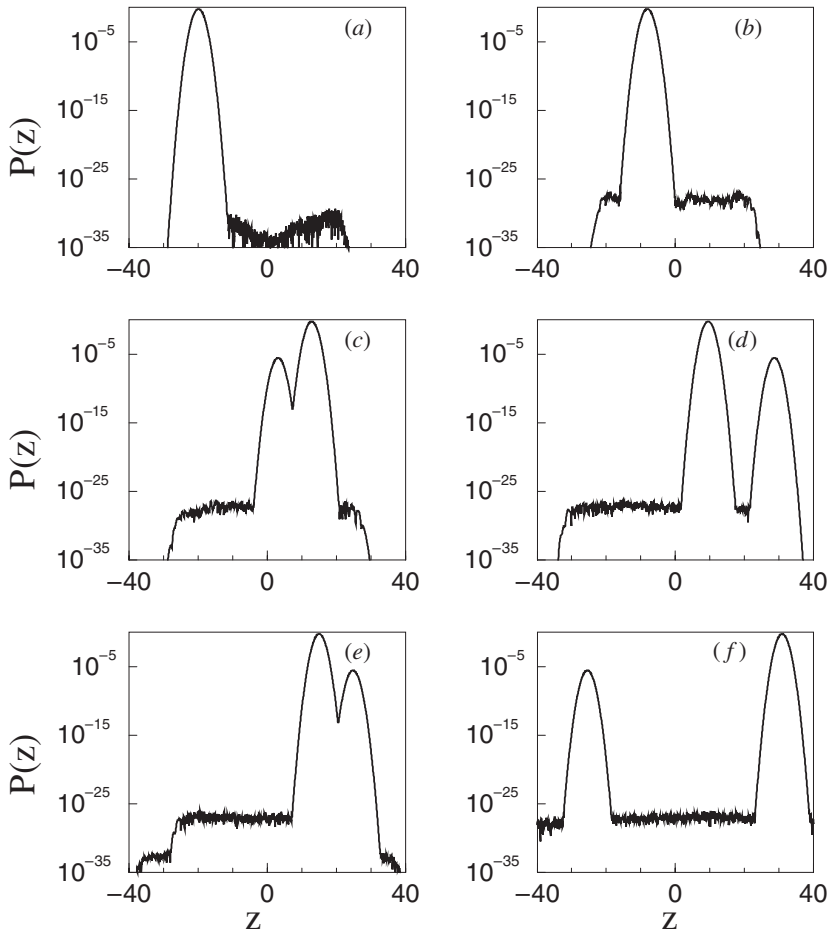

Figure 8. Probability distribution of the cantilever coordinate, z, for $\varepsilon = 400$ and $\eta = 0.3$. The initial conditions: $z(0) \equiv \langle z \rangle = -20$, $p_z(0) \equiv \langle p_z \rangle = 0$ ($\alpha = -\sqrt{2} \times 10$), and the average spin in the direction of the effective magnetic field.

So far, the described picture reminds us of the classical Stern–Gerlach effect in which the cantilever measures the spin component not in the z-direction but along the effective magnetic field. The appearance of the second peak, even if the average spin points initially in the direction of the effective magnetic field, provides a difference with the Stern–Gerlach effect. The origin of this peak is a small deviation from the adiabatic motion of the spin even at large amplitude of the effective field, and the back reaction of the cantilever vibrations on the spin.

5. Measuring a single-spin state

The next important question is the following: is it possible to use CAI MRFM not only to detect a spin signal but also to measure the state of a single spin? We studied numerically the phase of the cantilever vibrations when the initial spin points along or opposite to the direction of the effective magnetic field. Our computer simulations show that the phases of

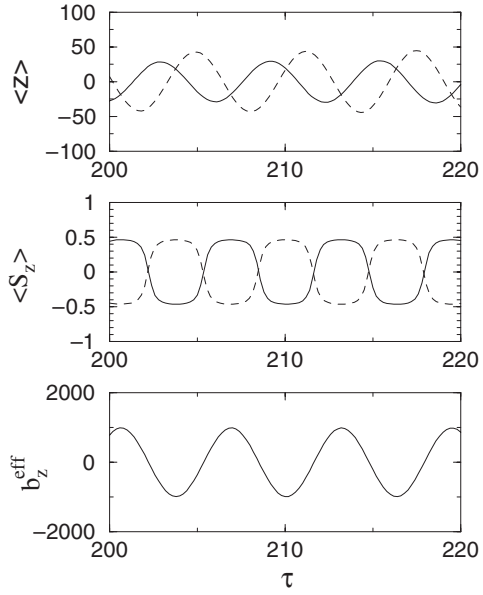

Figure 9. Measurement of the single-spin state using the phase of the cantilever vibrations. For the dynamics of $\langle z(\tau)\rangle$ and $\langle S_z(\tau)\rangle$ the solid line corresponds to the 'big' (classical) peak of the cantilever distribution, and the dashed line corresponds to the 'small' (quantum) peak, renormalized to similar amplitudes. At the bottom, the dynamics of the z-component of the effective field is shown.

the cantilever vibrations for these two initial conditions are significantly different. When the amplitude of the cantilever vibrations increases, the phase difference for two initial conditions approaches π. Thus, the classical phase of the cantilever vibrations indicates the state of the spin relative to the effective magnetic field.

In figure 9 we demonstrate the process of measurement of a single-spin state using the phase of the cantilever vibrations. For the dynamics of $\langle z(\tau)\rangle$ and $\langle S_z(\tau)\rangle$ the solid curve corresponds to the 'big' (classical) peak of the cantilever distribution, and the dashed curve corresponds to the 'small' (quantum) peak. At the bottom, the dynamics of the z-component of the effective field is shown. One can see that the solid curve of $\langle S_z(\tau)\rangle$ is in phase with the effective field component, $b_z^{\rm eff}(\tau)$. The phase difference of the cantilever vibrations corresponding to the two peaks approaches π for large enough times.

In practical applications, it would be very desirable to use CAI MRFM for measurement of the initial z-component of the spin. For this purpose, one should provide the initial direction of the effective magnetic field to be the z-direction. Then, the initial z-component of the spin will coincide with its component relative to the effective magnetic field. In our computer simulations presented in figures 4–7 we have assumed an instantaneous increase of the amplitude of the rf field, at $\tau = 0$. This causes an initial angle between the directions of the spin and the effective magnetic field, $\Theta \approx \epsilon/|{\rm d}\varphi/{\rm d}\tau| \approx 0.07$. To eliminate this initial angle we simulated the quantum spin–cantilever dynamics for an adiabatic increase of the rf field amplitude: $\epsilon = 20\tau$ for $\tau \leqslant 20$, and $\epsilon = 400$ for $\tau > 20$. The dependence for ${\rm d}\varphi/{\rm d}\tau$ was taken the same as in figures 4–7. The results of these simulations are qualitatively similar to those presented in figures 2–4, but the integrated probability of the small peak was reduced to its residual value $\sim 10^{-6}$.

We should also mention that the detection (without measuring the state) of a single electron spin in an atom can be used to determine the state of its nuclear spin [23, 24]. Such a measurement is possible for an atom with a large hyperfine interaction in a high external magnetic field, because the electron spin frequency of the atom depends on the state of its nuclear spin.

Certainly, for any single-spin measurement the amplitude of the driven cantilever vibrations must be greater than the amplitude of the thermo-mechanical noise. The amplitude of the driven cantilever vibrations for a single-spin detection can be estimated as $\eta Q_c Z_c$. The amplitude of the thermo-mechanical noise is presented, for example, in [14],

$$Z_{\rm rms} = 2[k_B T Q_c \Delta f / k_c \omega_c]^{1/2}$$

where Δf is the noise bandwidth. Thus, the minimum value of η for a single-spin measurement can be estimated as

$$\eta_{\rm min} \sim \omega^{-1} (k_B T \Delta f / \hbar Q_c)^{1/2}.$$

As an example, for the ultrathin cantilever reported in [25], with parameters

$$\Delta f = 0.4\,{\rm Hz} \qquad \omega_c/2\pi = 1.7\,{\rm kHz}$$

$$Q_c = 6700 \qquad k_c = 6.5 \times 10^{-6}\,{\rm N\,m^{-1}}$$

the value of $\eta_{\rm min}$ is

$$\eta_{\rm min} \sim 0.3\sqrt{T}.$$

For an electron spin this value corresponds to the magnetic field gradient (in tesla per metre),

$$(\partial B/\partial Z)_{\rm min} = 2\eta_{\rm min}(k_c \hbar \omega_c)^{1/2}/g\mu \sim 9 \times 10^4 \sqrt{T}$$

which is used in current experiments [26]. (Note that a detection of a single spin is connected with the driven vibrations of the cantilever, and does not depend on the specific initial conditions at the moment of 'turning on' the rotating magnetic field.)

The real problem of a single-spin detection is associated rather with the short spin relaxation time at the close distance of the cantilever to the measured spin [26]. In our estimation we assume that the spin relaxation time is greater than the time constant, t_c, of the cantilever. (For a cantilever reported in [25] this time is $t_c = Q_c/\omega_c \approx 0.6$ s.) This problem is awaiting solution.

We would emphasize that in this paper we did not discuss the exciting opportunity to detect a Schrödinger-cat state for a quasi-classical cantilever. Indeed, the decoherence time for such a state is very short. Following [27] the decoherence time, t_d, for a cantilever reported in [25] can be estimated as

$$t_d/t_c \sim \frac{\omega_c}{k_c k_B T}(\hbar/Z_{\rm rms})^2 = (\hbar\omega_c/2k_B T)^2(\omega_c/Q_c\Delta f) \approx 7 \times 10^{-15}/T^2.$$

Thus, for such 'macroscopic' parameters, the Schrödinger-cat state quickly transforms to a statistical mixture [30, 31] of two spin states relative to the directions of the effective magnetic field.

6. Summary

In conclusion, we have analysed the quantum effects in the single-spin measurement using cyclic adiabatic inversion (CAI) to drive cantilever vibrations in magnetic resonance force microscopy (MRFM). We investigated the quasi-classical cantilever interacting with a single

spin using the Hamiltonian approach. We have shown that the spin–cantilever dynamics generates two asymmetric peaks in the probability distribution of the cantilever coordinate corresponding approximately to the directions of the spin along or opposite to the direction of the effective magnetic field in the rotating frame.

We also have demonstrated that, in the regime of MRFM CAI, the cantilever measures the spin projection along the direction of the oscillating effective field in the rotating reference frame. When the components A and $\dot{\varphi}$ of the effective magnetic field in equation (24), that are responsible for CAI, are small in comparison with the effective field $\eta|z|$ (and, correspondingly, the conditions of CAI are violated) one will have a transition to the *standard* Stern–Gerlach experiment. Namely, the Hamiltonian (7) will be reduced to

$$\mathcal{H} = \left(p_z^2 + z^2\right)/2 - 2\eta z S_z \tag{26}$$

which has been considered in [28]. (Note that the model (26) can be considered as a modified Jaynes–Cummings model, see [29].) In this limit, the cantilever measures the projection of the spin in the direction of the magnetic field (z-direction). So, one can conclude that, depending on the system parameters, a cantilever is a device which measures the projection of the spin either in the direction of the oscillating effective field (MRFM CAI) or in the z-direction (Stern–Gerlach effect).

In this paper, we did not discuss the intriguing possibility of observing a Schrödinger-cat state. Instead, we concentrated on a possibility of observing the resonant excitation of the cantilever vibrations, driven by a single spin. We demonstrated by a direct computation of the average cantilever position and its standard deviation as a function of time that the resonant amplification of the cantilever oscillations is indeed possible (for the considered region of the system parameters), despite the presence of the two peaks for the cantilever distribution function. In fact, the standard deviation of the cantilever coordinate becomes large only when the angle between the initial spin direction and the effective magnetic field approaches $\pi/2$. In this case both peaks are approximately of equal size. However, after an observation of the cantilever position, the system appears in one of the peaks, and the following evolution of the cantilever coordinate shows again the resonant amplifications with a very small standard deviation.

The interaction of the cantilever with an environment will not change our main conclusion. Such an interaction will cause decoherence [30, 31], which transforms the linear superposition of the cantilever states into a statistical mixture. It is clear that this effect, as well as the thermal vibrations of the cantilever, cannot prevent an observation of the driven oscillations of the cantilever if the corresponding rms amplitude exceeds the amplitude of the vibrational noise. Another effect of the interaction with the environment is the finite quality factor, Q_c, of the cantilever, which puts the limit on the increase of the cantilever vibrations. The stationary amplitude of the cantilever vibrations can be estimated in our Hamiltonian approach by putting $\tau = Q_c$.

Finally, we mention two other possible techniques for the cyclic spin inversion in MRFM. One of them is the standard Rabi technique. This assumes that in our notation $\mathrm{d}\varphi/\mathrm{d}\tau = 0$ and $\epsilon = 1$, i.e. the Rabi frequency equals the cantilever frequency. This technique seems to be simpler than CAI MRFM. But the amplitude of the rf field, ϵ, must be much greater than the effective field produced by the cantilever on the spin $2\eta z \ll \epsilon = 1$. In this case, the force acting on the cantilever is very small, and the amplification of the driven cantilever vibrations requires a long time, i.e. a large cantilever quality factor. Another technique assumes the application of short π-pulses which periodically change the direction of the spin in the time interval, which is very short in comparison to the cantilever period [14]. If the time interval between successive pulses equals half of the cantilever period, this technique provides a resonant amplification

of the cantilever vibrations. Testing this technique in MRFM experiments is a challenging problem. Our results on numerical simulations of the 'short-pulsed' MRFM technique will be published elsewhere.

Acknowledgments

We thank H J Mamin, V Privman, D Rugar and J A Sidles for useful discussions. This work was supported by the Department of Energy under contract W-7405-ENG-36 and DOE Office of Basic Energy Sciences. The work of GPB and VIT was partly supported by the NSA, ARDA and DARPA (MOSAIC).

References

[1] Williams C P and Clearwater S H 1997 *Explorations in Quantum Computers* (Berlin: Springer)
[2] Berman G P, Doolen G D, Mainieri R and Tsifrinovich V I 1998 *Introduction to Quantum Computers* (Singapore: World Scientific)
[3] Lo H K, Popescu S and Spiller T (ed) 1998 *Introduction to Quantum Computation and Information* (Singapore: World Scientific)
[4] Pittenger A O 1999 *An Introduction to Quantum Computing Algorithms* (Basle: Birkhäuser)
[5] Braunstein S L (ed) 1999 *Quantum Computing* (New York: Wiley)
[6] Williams C P and Clearwater S H 2000 *Computing at the Quantum Frontier* (Berlin: Springer)
[7] Berman G P, Doolen G D and Tsifrinovich V I 2000 *Superlattices Microstruct.* **27** 89
[8] Kane B E 1998 *Nature* **393** 133
[9] Berman G P, Doolen G D, Hammel P C and Tsifrinovich V I 2000 *Phys. Rev.* B **61** 14694
[10] Berman G P, Doolen G D, Holm D D and Tsifrinovich V I 1994 *Phys. Lett.* A **193** 444
[11] Loss D and DiVincenzo D P 1998 *Phys. Rev.* A **57** 120
[12] Vrijen R, Yablonovich E, Wang K, Jiang H W, Balandin A, Roychowdhury V, Mor T and DiVincenzo D 1999 *Preprint* quant-ph/9905096
[13] Loss D, Burkard G and Sukhorukov E V 1999 *Preprint* cond-mat/9907133
[14] Berman G P and Tsifrinovich V I 2000 *Phys. Rev.* B **61** 3524
[15] Sidles J A 1991 *Appl. Phys. Lett.* **58** 2854
[16] Rugar D, Yannoni C S and Sidles J A 1992 *Nature* **360** 563
[17] Zhang Z, Hammel P C and Wigen P E 1996 *Appl. Phys. Lett.* **68** 2005
[18] Rugar D, Züger O, Hoen S, Yannoni C S, Vieth H M and Kendrick R D 1994 *Science* **264** 1560
[19] Rugar D, Stipe B C, Mamin H J, Yannoni C S, Stone T D, Yasumura K Y and Kenny T W 2001 *Appl. Phys.* A **72** (Suppl) S3
[20] Gurvitz S A 1997 *Phys. Rev.* B **56** 15215
[21] Korotkov A N 1998 *Preprint* quant-ph/9807051
[22] Morse P M 1948 *Vibration and Sound* (New York: McGraw-Hill) p 159
[23] Berman G P, Doolen G D, Hammel P C and Tsifrinovich V I 2000 *Phys. Rev.* B **61** 14694
[24] Berman G P, Doolen G D, Hammel P C and Tsifrinovich V I 2001 *Phys. Rev. Lett.* **86** 2894
[25] Stowe T D, Yasumura K, Kenny T W, Botkin D, Wago K and Rugar D 1997 *Appl. Phys. Lett.* **71** 288
[26] Stipe B C, Mamin H J, Stowe T D, Kenny T W and Rugar D 2001 *Phys. Rev. Lett.* **87** 6801
[27] Berman G P, Doolen G D, Hammel P C and Tsifrinovich V I 2002 *Phys. Rev.* A **65** 032311
[28] Berman G P, Borgonovi F, Lopez G V and Tsifrinovich V I 2002 *Preprint* quant-ph/0210006
[29] Jaynes E T and Cummings F W 1963 *Proc. IEEE* **51** 89
[30] Caldeira A O and Leggett A J 1985 *Phys. Rev.* A **31** 1059
[31] Zurek W H 1991 *Phys. Today* **44** 36